Final report on OTKA NN project 131270 “Holistic design of fuel cell electrocatalysts for the least power applications (CATALEAST)”

1. Main tasks of the project

Project CATALEAST, a consortium with complementary expertise in catalyst development and Polymer Electrolyte Membrane Fuel Cell (PEMFC) design, proposed development of novel composite-based corrosion resistant catalysts with improved stability and decreased Pt content; with subsequent integration of these materials into Membrane Electrode Assemblies (MEAs); and following studies of the MEAs in standard single PEM fuel cell and in new portable devices. A three membered international consortium has been formed: Research Centre for Natural Sciences **(P1)**, “Ilie Murgulescu” Institute of Physical Chemistry of the Romanian Academy **(P2)** and National Institute of Materials Physics **(P3)**. Moreover, the tasks regarding design, preparation and testing in portable fuel cell was done by involving Spanish partner **(CIEMAT)** as subcontractor.

Our goal was to find alternative catalysts to replace the corrosion-sensitive and expensive Pt/C electrocatalysts. A key element of our concept was the introduction of oxide materials, which would either act as catalysts by themselves, or partially or completely replace the carbon support. The previous experience of our research group was used to realize this concept by synthesizing anode Pt electrocatalysts with different Pt content supported on a conductive and corrosion resistant composite consisting of oxophilic metal M (M: W, Mo, Nb, Sn)-doped TiO_2 and various carbonaceous materials. In such a unique material system, the corrosion resistance and nanoparticle-stabilizing ability of TiO_2, the good co-catalytic properties of doping metals as well as the large surface area and high conductivity of active carbon are brought together. The transition metal dopant usually can facilitate the oxidation of CO at much lower potentials than on pure Pt, which is important when hydrogen from steam reforming is considered as fuel. Moreover, the Nb or Sn dopant is believed to promote the oxygen reduction reaction, thus e.g. Nb-doped TiO_2-carbon composites can be used at the cathode side.

Mesoarchitectured Pt-free PdRu catalysts supported on mesoporous WO_3 and SnO_2-WO_3 and their composites with graphene nanoplatelets (GNPs) prepared by **P2** were chosen as alternative anode catalysts. Nickel-based nanoarchitectural materials obtained by **P2** were proposed as one of the possible electrocatalysts for the cathode. Numerous novel catalytic systems were characterized by different physicochemical (**P2, P3**) and electrochemical methods (**P1**). The aims also included studies of the performance of MEAs with novel oxide-containing catalyst in single PEM fuel cell (**P1)** and in new portable fuel cell devices (**CIEMAT**).

2. Main results of the project

The research work in the project was performed in six work packages. Work Package 1 focused on the design and development of novel electrode materials. In this work package nickel-based nanoarchitectured materials as cathode and PdRu supported on mesoporous oxides and their composites as anode was prepared by **P2**. Using previous experience of our research group in the development of W-containing composite materials novel $Ti_{(1-x)}M_xO_2$-C (M: Mo, Nb, Sn; x= 0-0.4) mixed oxide and carbon composite supports and related Pt electrocatalysts were synthesized by **P1**. All members of consortium (**P1, P2, P3**) were involved in full characterization of new composite support materials and electrocatalysts by different physicochemical and electrochemical methods. In Work Package 2, we prepared MEAs with catalyst coated gas diffusion layer (GDL), and then tested these MEAs in a standard single PEM fuel cell. In Work Package 3, in the first phase, a Spanish subcontractor (**CIEMAT**) installed and tested portable single PEMFCs and stacks operating under full passive conditions using commercial gas diffusion electrodes. At the next stage, the best anode and cathode electrocatalysts developed within the project were also tested. In Work Package 4 for testing in single fuel cell, we have prepared the most promising electrocatalysts in the amount of 1 g for use as anode and cathode. As a result, the process of preparation of the three best anode and three best cathode catalysts was scaled up. Work Packages 5 and 6 included tasks related to dissemination and exploitation as well as project management.

2.1 Recent progress on electrocatalysts and electrodes for portable fuel cells- review

All members of the consortium contributed to a review entitled “Recent progress on electrocatalysts and electrodes for portable fuel cells” [1].

The utilization of fuel cells for portable electronic devices has seen remarkable increase in the last years. Performances of fuel cells, among others, strongly depend on the type electrocatalysts and membrane, anion exchange or cation exchange, used in the system. This review article [1] describes and discusses the state-of-the-art electrocatalysts used in the last years in different fuel cells: portable hydrogen–air fuel cells, direct methanol fuel cells, direct ethanol fuel cells and direct glycerol fuel cells. In addition, new electrode configurations for portable hydrogen micro fuel cells were also described.

Important to note is that the relationship between physicochemical properties and cell performances is decisive for the design of efficient electrocatalysts. Various catalysts with unique structures and morphologies, such as nanowires, nanosheets, and assembly structures, have been manufactured in recent years, and some of them show excellent catalytic performance characteristics.

2.2 Design and preparation of cathode electrocatalysts

In this project the design and development of novel electrode materials was planned. According to this at the cathode oxygen reduction reaction was planned to be catalysed with nickel-based nanoarchitectured materials ($NiWO_4$, $NiCo_2O_4$-SnO_2, Pt/$NiWO_x$) and their composites with graphene nanoplatelets (GNPs, which are hybrids between graphene and graphite). These materials were prepared by **P2** using innovative synthesis routes involving surfactants as templates to obtain mesoporous architecture. During the project, numerous variants of the synthesis of this type of catalysts were carried out under various reaction conditions using various surfactants and starting precursor compounds with different ratios between the components. The composition, structure and electrocatalytic activity of the best Pt catalysts supported on mesoporous $NiWO_4$ and $NiWO_4$-GNP composite are discussed in chapter 2.2.1. It should be noted that, regardless of the method of preparation and the presence or absence of GNPs, an attempt to replace Pt with Pd in $NiWO_4$-based catalysts leads to a decrease in catalytic activity.

Along with this, synthesis of $NiCo_2O_4$-SnO_2 was done by a self-assembly method using tripropylamine and diethanolamine as structural directing agents. Unfortunately, the activity of the $NiCo_2O_4$-SnO_2 catalyst materials remains negligible even after addition of the GNP.

Using the previous experience of our research group, Pt catalysts supported on Nb-containing mixed oxide–carbon composite were also recommended for use on the cathode side; details of the preparation and characterization of this catalytic system by various physicochemical and electrochemical methods are presented in chapter 2.2.2.

2.2.1 Pt catalysts supported on mesoporous $NiWO_4$ and $NiWO_4$-GNP composite

The results obtained on mesoporous $NiWO_4$, Pt/$NiWO_4$ and their composites with GNPs, used as bifunctional cathode and anode electrocatalysts, were recently published in ref. [2]. This article includes the design, preparation and detailed characterization of the best $NiWO_4$-based catalytic systems. The synergic phenomena between the $NiWO_4$ and GNP were induced by the direct synthesis route leading to a growth of $NiWO_4$ faceted crystallites with different W valence states (W^{6+}/W^{5+}).

Electrocatalytic performance of the catalysts was studied by *cyclic voltammetry (CV)* measurements. As shown in Fig. 1.a the presence of 8 wt.% of Pt in the samples reflected in some increase of the peak associated with adsorption of under potentially deposited hydrogen (H_{upd}) on Pt surface.

The electrocatalytic performance of the $NiWO_4$-based catalyst materials in the *oxygen reduction reaction (ORR)* (Fig. 1.b) and the *hydrogen oxidation reaction (HOR)* (Fig. 1.c) was evaluated by polarization curves measurements. Possibly, due to the low specific surface area (SSA= 22.4-25.4 m^2/g), the activity of carbon-free $NiWO_4$ and Pt/$NiWO_4$ catalysts was very low even at rotation speed of 1600 rpm. It should be noted that after carbon addition (Black Pearls 2000 (BP), CABOT), sizable increase of the ORR activity was observed only on the Pt/$NiWO_4$ catalyst (Fig. 1.b), but the activity of the Pt/$NiWO_4$-BP in the HOR remains negligible (Fig. 1.c). In this series of experiments, the best activity in the ORR and the HOR was obtained on the Pt catalyst supported on $NiWO_4$-GNP composite. The introduction of the GNPs resulted in changes in the crystalline framework as well as in the surface chemistry of the composite materials.

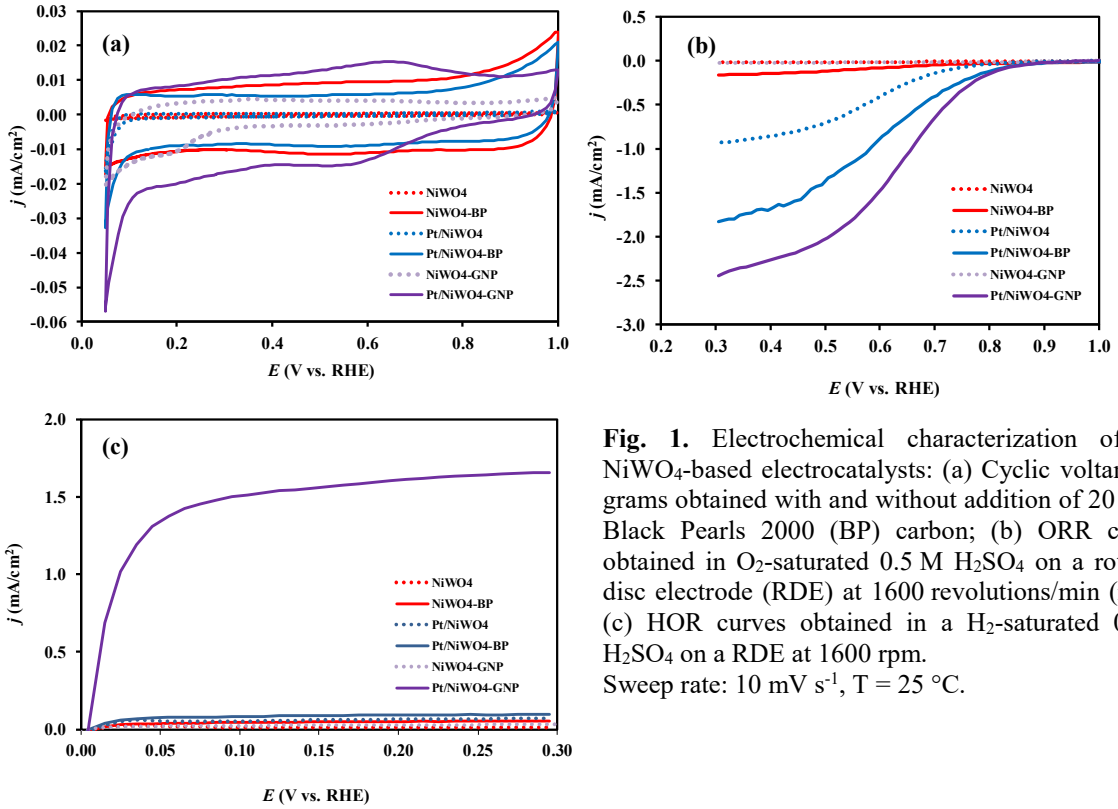

Fig. 1. Electrochemical characterization of the $NiWO_4$-based electrocatalysts: (a) Cyclic voltammograms obtained with and without addition of 20 wt.% Black Pearls 2000 (BP) carbon; (b) ORR curves obtained in O_2-saturated 0.5 M H_2SO_4 on a rotating disc electrode (RDE) at 1600 revolutions/min (rpm); (c) HOR curves obtained in a H_2-saturated 0.5 M H_2SO_4 on a RDE at 1600 rpm.
Sweep rate: 10 mV s^{-1}, T = 25 °C.

The activities expressed as mass specific current densities of the best 8 wt.% Pt/$NiWO_4$-GNP electrocatalyst and the commercial reference 20 wt.% Pt/C (QuinTech) in the ORR and the HOR were compared on Figs. 2.a and 2.b, respectively.

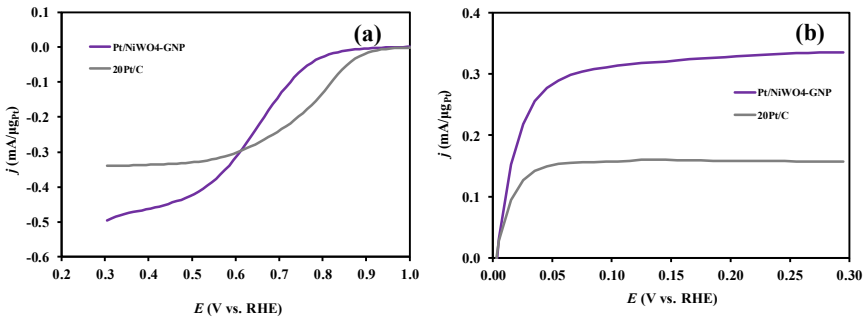

Fig. 2. Electrocatalytic performance of the 8 wt.% Pt/$NiWO_4$-GNP and reference 20 wt.% Pt/C (QuinTech) electrocatalysts in the ORR (a) and the HOR (b) measured in 0.5 M H_2SO_4 at 900 rpm in units of mass activity ($mA/\mu g_{Pt}$). *j* vs. *E* curves were obtained at 10 mV s^{-1} sweep rate. The Pt loading of the electrodes was 4.1 μg cm^{-2} and 10.2 μg cm^{-2} for Pt/$NiWO_4$-GNP and Pt/C catalysts, respectively.

Despite the fact that diffusion limiting current density of the Pt/$NiWO_4$-GNP sample was higher than that of the Pt/C catalyst (see Figure 2.a), the onset potential of the ORR was observed at less positive potential, indicating that this catalyst is less active. Moreover, as shown in Figure 2.a, the mixed kinetics-diffusion control region of the reference Pt/C (20 wt.% Pt; QuinTech) is in the range from 0.6 V and 1.0 V, but the diffusion-limited current density plateau was not reached on the composite supported catalyst, demonstrating that this catalyst does not perform well in the ORR.

The electron transfer number for the ORR was estimated from the slope of Koutecky - Levich plot: the obtained slope for theoretical $4e^-$ route (n= 4) is in good agreement with the value of the slope obtained experimentally for both electrocatalysts.

Conventionally, the Tafel analysis leads to two important physical parameters: the Tafel slope and the exchange current density. The results of the Tafel analysis performed for both catalysts were presented in Table 1. The similarity between the Tafel slopes shown in Table 1 suggests the same reaction mechanism on these two catalysts. As shown in Table 1, at a Tafel slope of ~-120 mV/decade,

the values of the exchange current densities, which depend not only on the Tafel slope, but also on the number of Pt sites involved, were 2.98×10^{-5} and 2.64×10^{-4} mA/cm^2 for the $NiWO_4$-based and reference catalysts, respectively.

Table 1. Tafel equations and calculated exchange current density values

Sample	Pt loading (μg cm^{-2})	Tafel equation / R^2	Tafel slope (mV/decade)	j_0 (mA/cm^2) [a]
8 wt.% Pt/$NiWO_4$-GNP	4.1	y = -0.1194x - 0.5403 R^2 = 0.9992	-119	2.98×10^{-5}
20 wt.% Pt/C [b]	10.2	y = -0.1222x - 0.4373 R^2 = 0.9964	-122	2.64×10^{-4}

[a] j_0: exchange current density, [b] reference electrocatalyst (QuinTech)

Figures 2.b display HOR voltammograms (positive-going scans) recorded via the RDE technique in H_2-saturated 0.5 M H_2SO_4 on the Pt/$NiWO_4$-GNP and 20 wt.% Pt/C electrocatalysts. On both polarization curves the steady-state current rises sharply from the origin with positive going potential and reaches a limiting plateau above 50 mV. As shown in Figure 2.b, the Pt mass specific current density of the HOR in the mixed kinetic-diffusion controlled region obtained on the Pt/$NiWO_4$-GNP catalyst was significantly higher comparing to the reference 20 wt.% Pt/C catalyst. Thus, the use of a new mesoporous $NiWO_4$-GNP composite as a support for Pt electrocatalysts has shown promising HOR activity, due most probably to the presence of both, WO_3 and $NiWO_4$, in this sample as revealed by XRD and XPS analysis. It has been assumed that the presence of defects and a special morphology of the $NiWO_4$-GNP facilitate the mass transfer of reactants to Pt active sites.

Rather similar slope 6.2×10^{-2} and 6.8×10^{-2} (mA/cm^2) rpm$^{-1/2}$ of Koutecky - Levich plot was obtained on the Pt/C and Pt/$NiWO_4$-GNP catalysts, respectively. These values are close to the theoretical value 6.54×10^{-2} (mA/cm^2) rpm$^{-1/2}$ obtained in 0.5 M H_2SO_4 for a smooth Pt electrode.

In additional experiments, we loaded $NiWO_4$-GNP composite materials with 20 wt.% Pt using our $NaBH_4$-assisted EG reduction-precipitation method. The activity of the 20 wt.% Pt/$NiWO_4$-GNP catalyst was high and quite similar to the activity of the reference 20 wt.% Pt/C catalyst.

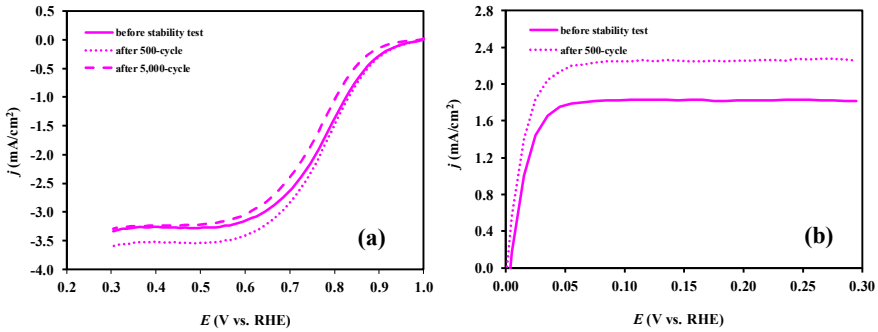

Fig. 3. Electrochemical characterization of the 20 wt.% Pt/$NiWO_4$-GNP catalyst recorded before (solid curves) and after 500 (dotted curves) and 5,000 (dashed curve) cycles of the stability test. (A) Oxygen reduction reaction curves obtained in O_2-saturated 0.5 M H_2SO_4 on a RDE at 900 rpm; (B) Hydrogen oxidation reaction curves obtained in a H_2-saturated 0.5 M H_2SO_4 on a RDE at 900 rpm. Sweep rate: 10 mV s^{-1}, T = 25 °C.

The effect of the 500- and 5,000-cycle stability test on the activity in the ORR and HOR was investigated (see Fig. 3). In this case the electrocatalytic performance of the $NiWO_4$-based electrocatalysts in the ORR and HOR was measured before and after stability test. As shown in Fig. 3.a after 500-cycle stability test the activity of the catalyst in the ORR increases and only very small decrease of the activity was observed after polarization for 5,000 cycles. These results indicate good corrosion resistance of the 20 wt.% Pt/$NiWO_4$-GNP catalyst.

The effect of the 500-cycle polarization on the activity in the HOR was studied using the same protocol as for ORR. Similar to the results obtained in the ORR, after the 500-cycle stability test the increase of activity in the HOR on the 20 wt.% Pt/$NiWO_4$-GNP catalyst was demonstrated (Fig. 3.b).

Thus, the peculiarity of this catalyst is some increase in the ORR/HOR activity after 500 polarization cycles, which can be attributed (i) to the formation of bimetallic nanoparticles or "Pt and metal oxide" ensemble sites upon the cyclic polarization, which provides a large promoting effect on the electrocatalytic performance, and/or (ii) to the cleaning of the electrode surface from residual impurities, which, if deposited on Pt, can cause a site-blocking effect.

Moreover, we loaded the $NiWO_4$ and $NiWO_4$-GNP composite materials with 8 wt.% Pt via our $NaBH_4$-assisted EG reduction-precipitation method. Although the reduction of Pt with $NaBH_4$ changes the surface structure of the mixed oxide to some extent, this deposition method provides a more dispersed Pt phase and, as a consequence, higher activity.

In additional experiments more complex composite support containing $NiWO_4$-GNP and $CePrO_x$ (Pr-doped CeO_2) with $NiWO_4$/GNP/$CePrO_x$ mass ratio of 70:20:10 was loaded with 16 wt.% of Pt using various Pt deposition methods. These catalysts show high activity in the HOR, which is comparable to the reference 20 wt.% Pt/C.

Our comprehensive structural and surface chemistry assessments indicate this composite material as a viable catalyst for PEMFCs using a broader type of fuels.

2.2.2 Pt catalysts supported on Nb-containing mixed oxide–carbon composite

According to the literature and our previous experience, the Nb-doped composites can be used as supports for electrocatalysts for the ORR.

Upon the preparation of $Ti_{(1-x)}Nb_xO_2$-C (x: 0.1-0.4; C: **BP**, Vulcan XC-72 (**V**); oxide/carbon ratios: 75/25 and 25/75) composites the success of the sol-gel-based multistep synthesis followed by high-temperature treatment (HTT: Ar, 600 °C, 8 h) was controlled by XRD. We demonstrated that exclusive incorporation of Nb in the TiO_2 is feasible only up to a certain solubility limit (below 10 atomic% Nb) during the high temperature treatment step of the synthesis, while excess Nb forms segregated surface oxides (see Table 2).

As shown in Table 2 in $Ti_{(1-x)}Nb_xO_2$-C ($x \geq 0.3$) composites the non-incorporated Nb formed an orthorhombic Nb_2O_5 phase. In the $Ti_{0.8}Nb_{0.2}O_2$-C sample, niobium pentoxide was not detected; nevertheless, the presence of amorphous or crystalline NbO_x phase below the detection limit cannot be excluded. According to the nitrogen adsorption measurements the increase of the Nb content in the composites resulted in slight increase of the S_{BET} of the support from 273 to 311 m^2/g (see Table 2).

Table 2. Structural properties of the composite materials determined by nitrogen adsorption measurements and XRD analysis

Nominal composition [a]	SSA [b] (m^2/g)	HTT [c] (Phase, %)			Lattice parameters, Å [d]	Nb subst., %	Size [e], nm	
		R	C	Nb_2O_5			R	Nb_2O_5
$Ti_{0.9}Nb_{0.1}O_2$-BP	273	70	25	-	a= 4.620, c= 2.970	7.8	20	-
$Ti_{0.8}Nb_{0.2}O_2$-BP	280	70	25	-	a= 4.620, c= 2.970	7.8	20	-
$Ti_{0.7}Nb_{0.3}O_2$-BP	299	70	25	5	a= 4.620, c= 2.970	7.8	18	12
$Ti_{0.6}Nb_{0.4}O_2$-BP	311	57	25	18	a= 4.620, c= 2.970	7.8	18	28
Nb_2O_5-BP	432	-	25	75	-	-	-	39
TiO_2-BP	236	75	25	-	a= 4.593, c= 2.959	-	43	-

[a] Expected composition of $Ti_{(1-x)}Nb_xO_2$ mixed oxide reflects desired Ti/Nb atomic ratio;
[b] SSA: the BET specific surface area;
[c] HTT: the samples were studied after HTT in Ar at 600 °C for 8 h;
[d] Lattice parameters of the rutile phase obtained after HTT; Pure rutile TiO_2: a= 4.593 Å, c= 2.959 Å;
[e] Average crystallite size of the rutile and Nb_2O_5 phases obtained after HTT;
R: rutile, C: carbon; in all cases the mass ratio of the oxide/BP carbon was 75:25.

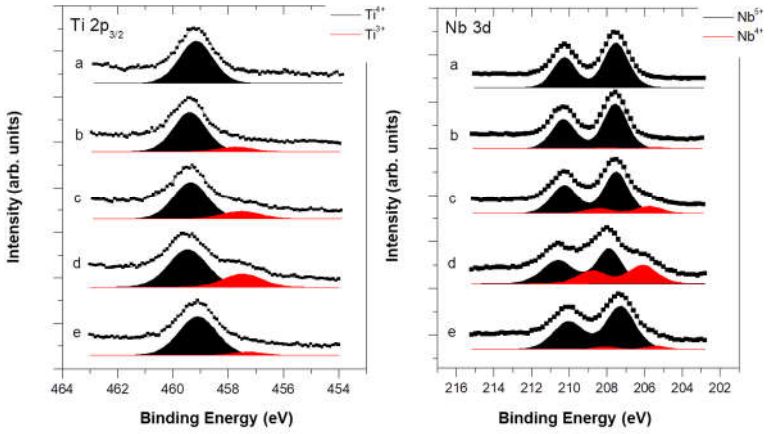

Fig. 4. Ti $2p_{3/2}$ and Nb 3d XPS spectra of the $75Ti_{0.7}Nb_{0.3}O_2$-25C composite obtained after different *in situ* treatments: (a) the sample was studied after sol-gel synthesis, before HTT; (b) the sample was studied after HTT in 300 mbar of Ar at 600 °C for 8 h; (c) the sample was studied after HTT in 10% H_2/Ar mixture at 600 °C for 2 h; (d) the sample was studied after HTT in Ar at 600 °C for 8 h and then reduced in 10% H_2/Ar mixture at 750 °C for 2 h; (e) after 16 hours of air exposure.

It appears from previous studies that a general feature of the doped (or undoped) TiO_2-carbon system is the tendency of the oxide for agglomeration, resulting in growth of large oxide particles. In particular, the HTT of the composite synthesis is assumed to be responsible for the agglomeration. Thus, decreasing the temperature of HTT may be a feasible way for preparation of better supports, but the appropriate temperature range (giving adequate incorporation) should be experimentally determined.

The changes in the oxidation state of Ti and Nb observed in the XPS spectra under different treatments on the $Ti_{0.7}Nb_{0.3}O_2$-C composite with oxide/carbon ratio of 75/25 were presented of Fig. 4. The surface composition/chemical state data were evaluated at each heating step. XPS results showed that bonding arrangements characteristic for the mixed oxide start to appear around a HTT temperature of 600–630 °C; but niobium at these temperatures is only partially incorporated; Nb still remains a predominantly surface species. A higher temperature of around 700-750 °C is required for the actual formation of the mixed oxide. At the same time, the apparent carbon content increases continuously during the annealing sequence, which means that agglomeration of the oxide starts even at relatively low temperatures. In fact, notable loss of oxide dispersion occurs at temperatures way below the onset of dopant incorporation, thus oxide agglomeration seems to be unavoidable if any form of HTT is needed. Similar composition changes were observed during the annealing treatments on the $Ti_{0.93}Nb_{0.07}O_2$ – BP carbon composite materials. Thus, this study demonstrated that decreasing of the temperature of HTT below 700 °C is not effective in preserving the oxide dispersion in the Nb-containing composites: agglomeration of the oxide phase is almost completed at these temperatures while the dopant still remains a surface species.

It should be noted that the ORR activity of the 20 wt.% Pt/$Ti_{(1-x)}Nb_xO_2$-C (x: 0.1-0.4) catalysts included in Table 2 decreases with increasing Nb content. The effect of the Pt loading (1, 5 and 20 wt.% Pt) on the electrocatalytic performance was also studied using $Ti_{0.7}Nb_{0.3}O_2$-C composite.

Based on the electrochemical results our Nb-containing composite supported catalysts were recommended for use on the cathode side (for details see chapter 2.4.2).

2.3 Design and preparation of anode electrocatalysts

At the anode side Pt electrocatalysts supported on a conductive and corrosion resistant composite consisting of transition metal (e.g. Mo, Sn)-doped TiO_2 and various carbonaceous materials (chapter 2.3.1) as well as mesoarchitectured Pt-free catalysts involving PdRu supported on mesoporous WO_3 and SnO_2-WO_3 mixed oxide and their composite with GNPs (chapter 2.3.2) were recommended as the most promising.

2.3.1 Pt catalysts supported on $Ti_{(1-x)}M_xO_2$-C (M: Mo, Sn; x= 0-0.4) composite

In case of Ti-Mo mixed oxide – carbon composites our efforts were aimed at optimizing the support or the Pt-loaded electrocatalyst by (i) selecting the type of carbonaceous materials, (ii) introducing its functionalization treatment, (iii) varying the mixed oxide/carbon ratio and (iv) introducing a post-synthesis reductive treatment. A side goal was to elucidate the nature of active Mo-Pt assemblies in mixed oxide-carbon $Ti_{0.8}Mo_{0.2}O_2$-C composite supports on the electrocatalytic performance of related Pt catalysts. The accumulated experience has opened up opportunities for the preparation of Mo-containing and Mo-free TiO_2-based composites containing novel carbonaceous materials. The results of this work were summarized in six publications [3-8].

Recently design of Pt electrocatalysts supported on $Ti_{(1-x)}Sn_xO_2$-C (x: 0.1-0.3) composite materials prepared by two different synthesis routes was also presented [9].

Mo-containing composite supported Pt catalysts

The multistep sol-gel synthesis of the $Ti_{0.8}Mo_{0.2}O_2$-C composite support materials with various mixed oxide/carbon mass ratio and preparation of electrocatalysts by loading them with 20 wt.% Pt was described in detail in ref. [3]. Experiments with systematic variation of the oxide/carbon ratio in the composite revealed that a slight adjustment of the synthesis procedure is needed in the duration and temperature of the aging step, as well as in the pH control before the aging procedure in the case of systems with high carbon content. An optimized synthesis route was elaborated for composites containing Vulcan, exfoliated graphite oxide (GO), unmodified BP and functionalized Black Pearls 2000 (F-BP) carbon materials.

The details of the functionalization of commercial BP carbon performed by either a one-step treatment with glucose or by a two-step treatment with HNO_3 and glucose can be found in ref. [4]. The influence of the pre-treatment of carbon in nitrogen at 1000 °C for 3 h before functionalization was also demonstrated [4].

GO can be considered as an extreme case of functionalized carbon materials. Due to its extremely high content of functional group, its exfoliation and handling in sol-gel synthesis is much easier than that of other, more hydrophobic new types of carbonaceous material (i.e. mono- and multi wall carbon nanotubes, graphene, etc.). Our previous method for the preparation of the $Ti_{1-x}Mo_xO_2$-active carbon composite type of electrocatalyst support was successfully adapted to the use of GO starting material [3]. Recently, the peculiarities of the preparation of GO derived composites have been demonstrated using the example of Mo-free TiO_2-GO [5]. The structural and compositional properties of the composite materials and Pt catalysts were studied by XRD, XPS, TEM, SEM/EDX and N_2 adsorption measurements. It was proved by XRD measurements that addition of 5 hours aged solution of Ti(O-*i*-Pr)$_4$ to GO delaminated by means of NaOH solution under vigorous stirring resulted in exclusively rutile-TiO_2 phase after HTT. As GO is known to be thermally unstable, we studied the changes of the carbonaceous component during the preparation of the composite. Based on literature data we supposed that the destruction of the GO plates could be reduced by solvothermal treatment. Therefore, a new solvothermal treatment in *i*-PrOH was involved into the procedure prior to HTT (Ar, 600 °C, 8 h).

$Ti_{0.8}Mo_{0.2}O_2$-C composites with 25 wt.% GO and rutile-TiO_2 structure were also prepared by a slightly altered synthesis procedure [3]. The problem is that crystallized $NaNO_3$ appears in the presence of NaOH used for the delamination of GO at the end of the first step of our conventional multi-step sol-gel composite preparation method. Unfortunately, $NaNO_3$ decomposes leading to uncontrolled treatment conditions under HTT needed to incorporate Mo into the rutile-TiO_2 phase. Therefore, the liquid phase in the slurry had to be changed and the solid part had to be washed with diluted nitric acid in order to remove the well soluble $NaNO_3$ before addition of the Mo precursor. XRD and XPS measurements proved that using this procedure $NaNO_3$ could be removed before HTT.

As demonstrated by XRD, using the optimized synthesis route, despite the very different structural and surface chemistry of the carbon materials comparing to the samples obtained without solvothermal treatment, the rutile structure of the mixed oxide was maintained and almost complete Mo incorporation was achieved. GO-derived composites with S_{BET}= 100-300 m^2/g were loaded with 20 wt.% of Pt by a $NaBH_4$-assisted ethylene glycol reduction-precipitation method. The effect of an additional solvothermal treatment on the structure, catalytic activity and stability of Pt electrocatalysts was demonstrated.

It should be emphasized that the accumulated experience has opened up opportunities for the preparation of TiO_2-based composites containing novel carbonaceous materials, such as GNPs,

multilayer graphene (MG) and N-doped graphene. Moreover, a relatively simple and promising method for producing this type of composites using a ball milling technique has been developed. Comparing the electrochemical behavior of Pt catalysts supported on TiO_2-C composites synthesized by different methods, the ball-milled MG-containing sample has lower the ECSA and activity than Pt/TiO_2-GO derived catalyst and the commercial Pt/C. However, it should be noted, the stability of both new types of samples is higher than that of commercial Pt/C [6].

These observations will form the base for the PhD theses "Novel electrocatalysts for PEM fuel cells by use of new type of carbonaceous materials: preparation and characterization" of Ilgar Ayyubov, who is a PhD student of the George Oláh Doctoral School of Budapest University of Technology and Economics.

Our recent studies have demonstrated improved stability of Mo-containing composite supported catalysts over a wide range of potentials/pH with respect to Pt/C systems, along with enhanced resistance to CO [3,4]. Electrochemical studies pointed out that the sites of the catalysts responsible for CO tolerance are formed between Pt and reducible Mo species on the surface of the composite support [3]. The EDX elemental maps of the Pt/$Ti_{0.8}Mo_{0.2}O_2$-F-BP catalyst with $Ti_{0.8}Mo_{0.2}O_2$/C= 75/25 ratio, presented in Fig. 5, show a homogeneous distribution of the Ti and Mo elements over the mixed oxide particles, indicating that the desired mixed oxide-carbon composite structures were successfully formed. Moreover, in the map demonstrating distribution of the Pt and Mo elements the presence of Pt NPs surrounded with Mo was observed [7]. It should be noted that the presence of Mo in close vicinity to Pt is one of the key requirements of the increased CO tolerance [3, 7].

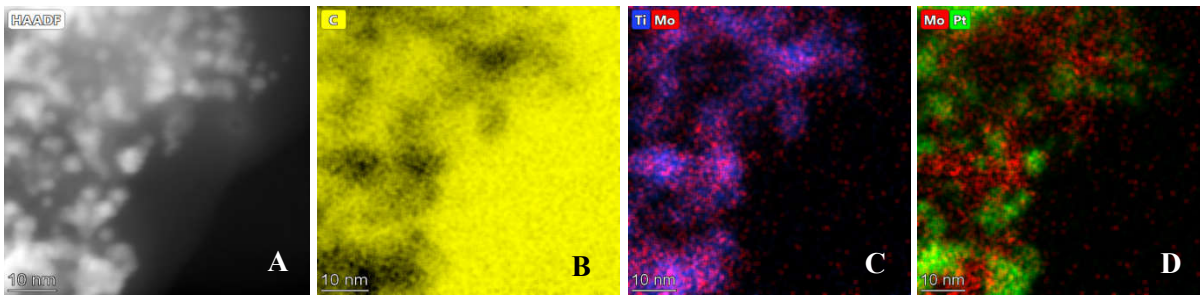

Fig. 5. Elemental maps of the 20 wt.% Pt/75 wt.% $Ti_{0.8}Mo_{0.2}O_2$-25 wt.% F-BP catalyst.

The electrochemical results indicate that (i) there are characteristic performance differences between the electrocatalysts with different mixed oxide/carbon ratio, and (ii) the catalytic properties of the system are mainly determined by the Pt-Mo interactions [3, 7]. Thus, an increase of the mixed oxide content in composites, leading to a pronounced enhancement of Pt-Mo interactions, results in better tolerance of the catalysts to CO as compared to those with high carbon content. However, the more homogeneous microstructure of the catalysts with high carbon content (75 wt.%) seems to be the key for enhanced long-term stability.

These results were used in the BSc theses "Preparation of novel composite support materials for CO tolerant and stable anode electrocatalysts" of Khirdakhanim Salmanzade presented at the Budapest University of Technology and Economics in 2020.

Considering also the fact that high oxide content in the catalyst layer can lead to a slight increase of the cell resistance, the BP- and F-BP-based Pt electrocatalysts with $Ti_{0.8}Mo_{0.2}O_2$/C= 25/75 ratio seems to be more promising for general use: the smallest performance loss was observed on the catalyst prepared using F-BP carbon (7% ECSA loss after 500 and 24% after 10,000-cycle stability test) [3].

In order to clarify the possibility of using these catalysts as anode or cathode in PEM fuel cells, their performance in the HOR and the ORR was also investigated (see chapter 2.4.1).

Pt and the mixed oxide form a couple liable for strong metal-support interaction (SMSI) phenomenon, generally manifesting itself in decoration of the metal particles by ultrathin layers of the support material upon annealing under reductive conditions. In order to induce SMSI, effect of the reductive treatment at 250 °C on the state and electrocatalytic behavior of Pt in catalysts supported on $Ti_{0.8}Mo_{0.2}O_2$-BP composite ($Ti_{0.8}Mo_{0.2}O_2$/C= 50/50) was recently investigated [8]. X-ray photoelectron spectroscopy (XPS) measurements combined with *in situ* H_2 exposure experiments were performed on

the reduced catalyst in order to obtain information about the details of the interaction between the oxide and the Pt particles.

The electrochemical experiments pointed out a small loss of the electrochemically active surface area (ECSA) of Pt with respect to the original catalyst, while XPS suggested only a minimal decrease of the Pt dispersion. At the same time, hydrogen exposure experiments combined with XPS on the reduced catalyst demonstrated the presence of a Mo species very easily reducible to the metallic state, which we previously interpreted as Mo directly adsorbed on the Pt surface. No such behavior was observed for Ti. Accordingly, even if Mo remains support-bound in the original catalyst, the reductive treatment at 250 °C is enough to induce a partial encapsulation of the Pt particles with a Mo-containing overlayer, which explains the decrease of the electrochemically active surface area (ECSA). On the other hand, probably due to the presence of Mo-containing species on Pt, enhanced stability of the reduced catalyst was demonstrated by 10,000-cycle stability test.

Thus, the results of this preliminary study confirmed that utilization of the SMSI phenomenon can indeed be a valuable approach for improving the stability of the mixed oxide – carbon composite supported electrocatalysts.

These observations will form the base for the PhD theses "Assessment of the role of strong metal support interaction (SMSI) on electrocatalytic performance of supported Pt catalysts" of Maria Cristina Silva Cisneros, who is a PhD student of the George Oláh Doctoral School of Budapest University of Technology and Economics.

Sn-containing composite supported Pt catalysts

The synthesis of novel $Ti_{(1-x)}Sn_xO_2$-BP (x: 0.1-0.3) composite supports for Pt electrocatalysts with oxide/carbon ratio of 75/25 was developed using various Sn precursor compounds: tin (II) oxalate ($Sn(C_2O_4)$) and tin (IV) chloride pentahydrate ($SnCl_4 \times 5H_2O$).

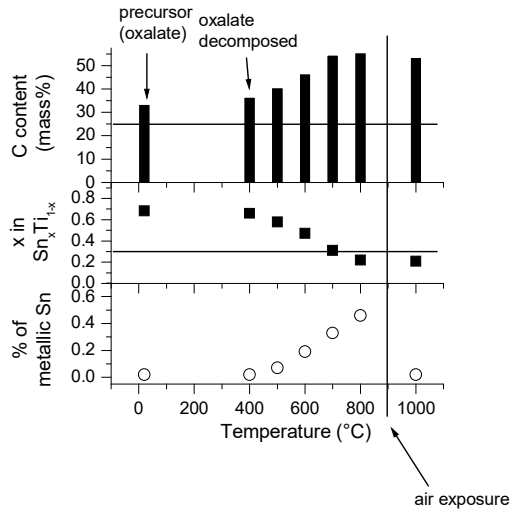

Fig. 6. Influence of different treatments on the Ti/Sn ratio, weight percentage of the carbonaceous material as well as the Sn^0 content calculated from XPS measurements of the $Ti_{0.8}Sn_{0.2}O_2$-BP composite material with oxide/carbon ratio of 75/25 prepared using $Sn(C_2O_4)$.

As shown in Fig. 6, according to the XPS results, the apparent carbon content of the $Ti_{0.8}Sn_{0.2}O_2$-BP composite prepared using $Sn(C_2O_4)$ and dried at 85 °C was about 33 wt.%; the Ti/Sn ratio significantly exceeded the calculated value (corresponding to $Ti_{0.32}Sn_{0.68}$), which probably means that highly dispersed tin-containing species uniformly cover the surface of the sample. After decomposition of the Sn precursor (above 400 °C) a gradual decrease of tin content is observed until, after 700 °C heat treatment, the tin content stabilizes near the nominal value ($Ti_{0.79}Sn_{0.21}$). An increase of the temperature of heat treatment in vacuum to 800 °C leads to the reduction of some part of tin to the metallic state; however, exposure to air for 16 h results in the complete oxidation of Sn^0 to SnO_2. This HTT also results in some sintering of the mixed oxide phase and, as a consequence, to an increase in the carbon content

up to 55 wt.%. From the evaluation of the compositional data, quantities such as the Ti/Sn ratio, weight percentage of the carbonaceous material as well as the Sn^0 content were derived and presented in Fig. 6.

Based on the XRD results after HTT, the samples prepared using $SnCl_4 \times 5H_2O$ according to an adapted method developed for Mo-containing composites consist of rutile crystallites and metallic Sn in a small amount (1-2%). The degree of incorporation of Sn increased with the amount of the tin precursor compound added during the synthesis (Sn_{subst} was 7, 14 and 23% for $Ti_{(1-x)}Sn_xO_2$-C composite with x: 0.1, 0.2 and 0.3, respectively). It should be noted that after the deposition of Pt, the reflections of the metallic Sn completely disappear; in all Pt catalysts, platinum is present in nanodispersed form. However, electrocatalysts obtained using this preparation route had unusually low ECSA (~30 m^2/g_{Pt}). This is especially strange since according to the N_2 adsorption measurements, the SSA of Sn-containing samples was even higher compared to the Mo-containing composites with oxide/carbon ratio of 75/25 (S_{BET}= between 373-438 m^2/g and 248 m^2/g for $Ti_{(1-x)}Sn_xO_2$-BP, and $Ti_{0.8}Mo_{0.2}O_2$-BP respectively).

To avoid these shortcomings, the synthesis of the Sn-containing composite was modified [9]: the precursors of Sn and Ti were introduced simultaneously at the beginning of the synthesis, before the addition of carbon and the aging step. This became possible due to the fact that SnO_2 crystallizes in the rutile phase. We demonstrated that the composites and Pt electrocatalysts obtained using this preparation route had the following advantages comparing to samples prepared using our traditional synthesis method [9]: (i) the formation of Sn^0 or SnO_2 was not observed either by XRD or by XPS; (ii) based on TEM results the supports have a more homogeneous/uniform mixed oxide distribution, and (iii) ECSA values were comparable to those obtained on Mo-containing composites of similar composition.

In order to clarify the possibility of using the Sn-containing Pt/$Ti_{(1-x)}Sn_xO_2$-C catalysts (x: 0.1-0.3) as anode or cathode in PEM fuel cells, their electrocatalytic characteristics were investigated. A sharper increase in the HOR current observed on Sn-containing platinum catalysts compared to Pt/C indicates the efficiency of this catalytic system. Based on the electrochemical results, it was concluded that the behavior of electrocatalysts mainly depends on the synthesis route used in the preparation of the composite support materials and does not depend on the Ti/Sn ratio.

These results were used in the MSc theses "Preparation of novel composite support materials for CO tolerant and stable anode electrocatalysts" of Khirdakhanim Salmanzade presented at the Budapest University of Technology and Economics in 2022. Moreover, these results were presented at the 13th International Symposium of the Romanian Catalysis Society (RomCat 2022; Baile Govora, Romania, June 22-24, 2022) [9] and planned to be published after the conference in the Special Issue of the Catalysis Today journal.

2.3.2 PdRu electrocatalysts supported on mesoporous WO_3 and SnO_2-x%WO_3 (x: 10-30 mol.%) mixed oxide and their composite with GNPs

Synthesis of PdRu electrocatalysts supported on GNP-containing WO_3 and SnO_2-x%WO_3 (x: 10-30 mol.%) oxide-based composite materials using various synthesis routes was done by **P2.**

Sizable increase of the HOR activity was observed on the mesoporous SnO_2-x%WO_3 (x: 10 and 30 mol.%) materials with high dispersion of tungsten into SnO_2 matrix prepared using a hydrothermal synthesis route with a non-ionic surfactant Brij 52 only after dispersion of 10 wt.% Pd and 10 wt.% Ru in the oxide matrix. However, the effect of Ru on the activity of catalytic systems containing different amounts of WO_3 in composite materials was not unambiguous. The activity of the PdRu/SnO_2-10%WO_3 catalyst was higher compared to the samples containing only Pd; and vice versa, the addition of Ru to the Pd/SnO_2-30%WO_3 catalytic system resulted in activity decrease. The use of another surfactant, Triton X100, in the preparation of composite materials does not lead to significant changes in the HOR activity.

Compared to these catalytic systems, a significant increase in the HOR activity was obtained on Pd catalysts supported on composites of RuO_2-WO_3-SnO_2 oxides and GNP, prepared by direct synthesis using cotton fibers as a template. Cotton fibers used as a template provide mesoporous stricture of composite materials. High activity with unusual form of polarization curve was obtained on the electrocatalyst with 10 wt.% of Pd loading supported on RuO_2-30%WO_3-GNP composite.

2.4 Scale-up of the preparation of the best composition

2.4.1 Electrochemical characterization of the scaled-up 20 wt.% Pt anode catalysts in a standard three-electrode cell

According to the half-cell results presented in ref. [3], the most promising anode electrocatalysts were the 20 wt% Pt-containing $Ti_{0.8}Mo_{0.2}O_2$-C type composite supported systems. From this family, the most stable three catalysts with $Ti_{0.8}Mo_{0.2}O_2$/C= 25/75 mass ratio prepared using Vulcan, BP and F-BP as carbon materials were selected for use as anode catalyst in PEM fuel cell experiments.

As shown in our recent study [10], the developed preparation method makes it possible to obtain about 1 g of composite material in one batch. To ensure that the synthesis was successful, prior to Pt deposition, the $Ti_{0.8}Mo_{0.2}O_2$-C composites were characterized by powder X-ray diffraction (XRD) and nitrogen adsorption measurements. The results of physicochemical characterization of the unified materials are summarized in Table 3. Comparison of these results with our previous ones presented in the ref. [3] demonstrates a good reproducibility of the synthesis. Our recent experiments have shown that, using our multi-step sol-gel synthesis method, subsequent increases of the amount of mixed oxide – carbon composite support materials produced in one batch can be easily carried out.

Table 3. Physicochemical and electrochemical characterization of the $Ti_{0.8}Mo_{0.2}O_2$-C (C: Vulcan, BP and F-BP) composite supports and the related Pt catalysts

Sample [a]	BET surface area, m^2g^{-1} [b]	Pore volume, cm^3g^{-1}	Rutile lattice parameters, Å [c]	Pt size, nm (XRD)	$ECSA_1$, [d] m^2/g_{Pt}	$\Delta ECSA_{10,000}$, % [e]
Pt/75BP	1120	2.01	a= 4.630, c= 2.940	2.68	69.7 ± 2.6	27.6
Pt/75F-BP	726	1.32	a= 4.630, c= 2.940	2.75	70.9 ± 1.6	24.1
Pt/75V	175	0.48	a= 4.630, c= 2.940	2.08	78.3 ± 2.6	36.4

[a] BP: Black Pearls 2000, F-BP: functionalized BP (carbon pre-treated at 1000°C in N_2 for 3 h before functionalization, then functionalized with HNO_3 and glucose), V: Vulcan;
[b] Specific surface area of the composite support materials determined by nitrogen adsorption measurements;
[c] Lattice parameters of the rutile phase obtained after HTT; pure rutile TiO_2: a= 4.593 Å, c= 2.959 Å;
[d] The average values of the ECSA obtained on fresh catalysts for five different batches;
[e] $\Delta ECSA_{10,000}$ was calculated from the charges originated from the hydrogen desorption in the 1st and 10,000th cycles: $\Delta ECSA_{10,000}$= {1-($ECSA_{10,000}$/$ECSA_1$)}×100%.

Composite support materials were loaded with 20 wt.% Pt via a modified $NaBH_4$-assisted ethylene-glycol reduction-precipitation method, which has been proved to result in highly dispersed Pt nanoparticles with average particle size of ~ 2 nm on the surface of our composites even at high Pt load (up to 40 wt.%).

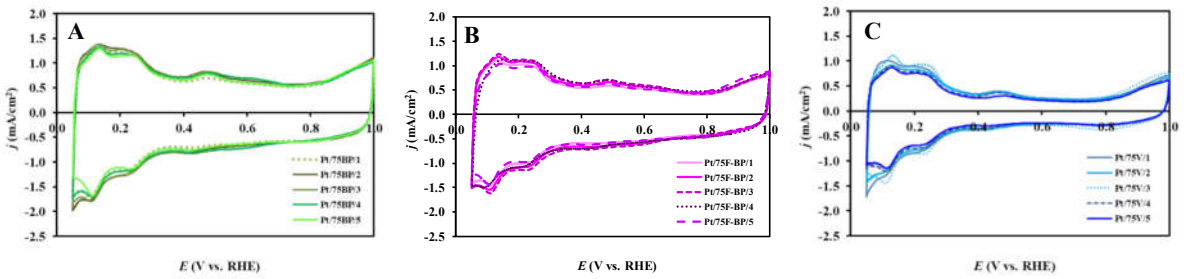

Fig. 7. Electrochemical characterization of various batches of Pt electrocatalysts by cyclic voltammetry: (A) Pt/75BP, (B) Pt/75F-BP and Pt/75V (C). Cyclic voltammogram recorded in 0.5 M H_2SO_4 at 100 mV s^{-1}, T = 25 °C.

The Pt-loading method gave the best results (in term of Pt dispersion and uniformity) with 0.2 g of composite support material in one run. An appropriate amount of electrocatalysts sufficient for detailed characterization by various techniques as well as for the measurements in standard single and portable fuel cells has been obtained in four – five batches. Characterization of different batches of Pt electrocatalysts by cyclic voltammetry was done before unifying them (see Fig. 7). Fig. 7 confirms the good reproducibility of the Pt loading obtained for different batches.

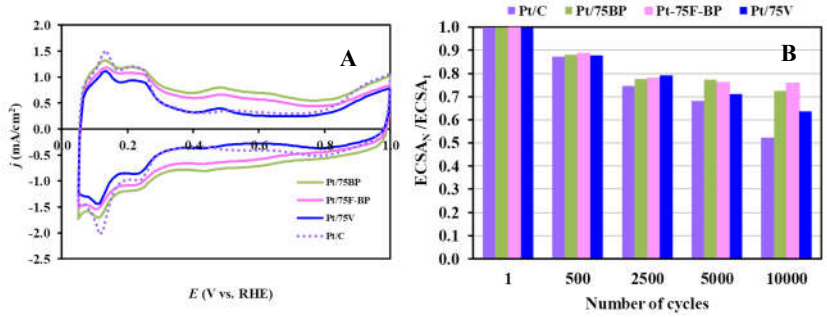

Fig. 8. Cyclic voltammograms of the 20 wt.% Pt/75$Ti_{0.8}Mo_{0.2}O_2$-25C electrocatalysts (A) and the results of the electrochemical long-term stability test (B): comparison of the electrochemically active Pt surface area measured after N cycles normalized to ECSA measured in the 1st cycle ($ECSA_N/ECSA_1$) of the Pt/75BP (green), Pt/75F-BP (pink) and Pt/75V (dark blue) catalysts as a function of the number of cycles (N); results obtained on the reference Pt/C catalyst (violet) is given for comparison. Recorded in 0.5 M H_2SO_4 at 100 $mV \cdot s^{-1}$, T= 25 °C.

Comparison of cyclic voltammograms obtained on the reference Pt/C and three 20 wt.% Pt/75$Ti_{0.8}Mo_{0.2}O_2$-25C electrocatalysts was presented in Fig. 8.A. A typical cyclic voltammogram of Pt with the classical features of the adsorption/desorption of underpotentially deposited hydrogen between 50 and 350 mV along with a redox peak pair of the Mo between 380 and 530 mV was observed on the all studied composite supported Pt catalysts (see Fig. 8.A). The appearance of these redox peaks in the voltammograms clearly confirm that there is an active interface between the Pt nanoparticles and the surface Mo species of the composite support. It should be noted, that, as shown in Fig. 8.A, the extent of the double layer capacity between 400 mV < E < 600 mV depends on the type of carbonaceous materials used for the preparation of the catalysts and correlates well with the BET surface area of the composite materials calculated on the base of N_2 adsorption measurements (see Table 3).

As shown in Table 3, our reduction-deposition method applied for Pt deposition results in highly dispersed nanoparticles with an average Pt size of about 2-3 nm. In order to demonstrate the reproducibility of sample preparation, Table 3 also includes the average values with the corresponding standard deviation of the electrochemically active Pt surface area obtained after the cleaning procedure in the first cycle for five different batches on each composite supported catalyst.

As shown in Table 3, the $\Delta ECSA_{10,000}$ values confirm the higher stability of the BP-containing catalysts, which, as demonstrated in our recent study [3], can be explained by the more homogeneous microstructure of the catalysts with high content of the high specific surface area carbonaceous starting material. However, as can be seen from Figure 8.B, this difference in stability between these catalysts only begins to appear after 5,000 cycles of the stability test.

In our recent study [10] the electrocatalytic activity of the scaled-up catalysts in the HOR and in the ORR were compared with a commercial Pt/C reference catalyst by rotating disc electrode (RDE) technique: the performance in the ORR and the HOR expressed as current values normalized to the geometric surface area of the electrode was compared in Fig. 9.

As shown in Figure 9.A, current density of the ORR in the mixed kinetic-diffusion controlled region, where the rate of the ORR reaction is limited by the availability of oxygen at the electrode surface, was higher on the fresh reference Pt/C catalyst compared to the composite supported Pt catalysts; identical diffusion limited currents were reached on the Pt/75F-BP and Pt/75V catalysts, whereas the limiting current of the Pt/75BP catalyst was slightly higher which may be due to the different morphology of the support. Smaller limiting current density observed on oxide-containing can be originated from slower diffusion of O_2 through the oxide layer covering the Pt nanoparticles.

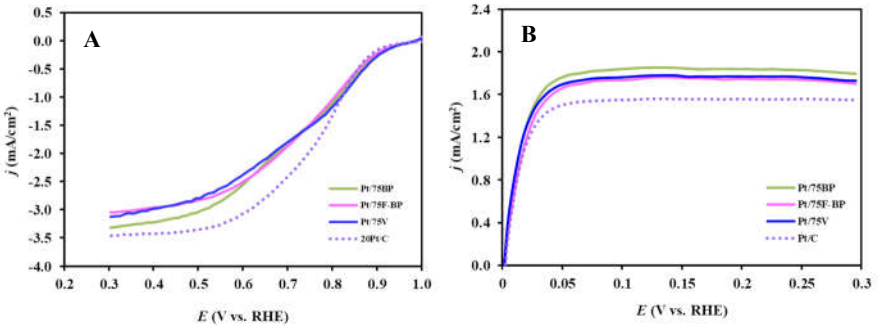

Fig. 9. Electrochemical characterization of the reference Pt/C (violet) and Mo-containing composite supported Pt catalysts by RDE measurements at 900 rpm: Pt/75BP (green), Pt/75F-BP (pink) and Pt/75V (dark blue). (A) ORR curves obtained in O_2-saturated 0.5 M H_2SO_4; (B) HOR curves obtained in a H_2-saturated 0.5 M H_2SO_4. Obtained at 10 mV s^{-1}, T= 25 °C

The kinetic parameters related to ORR performance determined using Koutecky-Levich (K-L) plot suggested 4-electron transfer per oxygen molecule leading to the formation of H_2O. The similarity between the Tafel slopes suggested the same reaction mechanism for these electrocatalysts.

The efficiency of the composite-supported electrocatalysts in the HOR was independent of the type of carbonaceous material used, while the reference Pt/C catalyst showed slightly lower limiting current density. The slope of the K-L plots was rather similar and close to the theoretical value: 6.2×10^{-2} and 7.1×10^{-2} (mA/cm^2) rpm$^{-1/2}$ on the V-containing (Pt/C and Pt/75V) and BP-containing (Pt/75BP and Pt/75F-BP) catalysts, respectively.

2.4.2 Electrochemical characterization of the scaled-up 40 wt.% Pt cathode catalysts in a standard three-electrode cell

According to the half-cell results, three catalysts loaded with 40 wt% Pt were selected for use as cathode catalyst in PEM fuel cell experiments: Pt/$NiWO_4$-GNP, Pt/75$Ti_{0.93}Nb_{0.07}O_2$-25BP and Pt/25$Ti_{0.93}Nb_{0.07}O_2$-75V.

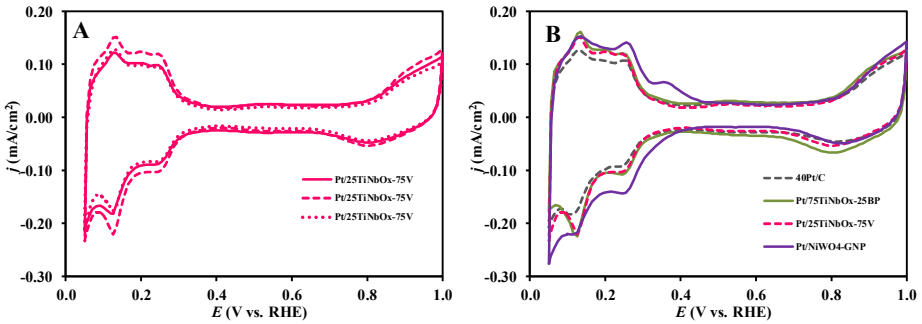

Fig. 10. (A) Electrochemical characterization of various batches of 40 wt.% Pt/25 wt.% $Ti_{0.93}Nb_{0.07}O_2$-75 wt.% V catalyst by cyclic voltammetry; (B) Comparison of cyclic voltammograms of the 40 wt.% Pt catalysts. Obtained in 0.5 M H_2SO_4 at 100 mV s^{-1}, T = 25 °C.

Pt loading on the most promising cathodic catalyst supports (0.2 g) was carried out in a similar way as described for anodic catalysts. Thus, in the case of the 40 wt.% Pt loading, the appropriate amount of electrocatalyst (1 g) was obtained in three batches. Characterization of different batches of Pt catalysts by cyclic voltammetry measurements (see Fig. 10.A) shows good reproducibility of the Pt loading.

Comparison of cyclic voltammograms of the 40 wt.% Pt catalysts was presented in Fig. 10.B. As shown in Fig. 10.B, all catalysts studied show a typical CV of Pt with the classical features of the underpotentially deposited hydrogen desorption between 50 < E < 400 mV. Moreover, a characteristic feature of the voltammogram obtained on the Pt/$NiWO_4$-GNP is the asymmetry in the so-called hydrogen region: there is quite pronounced peak in the anodic branch of the voltammogram above 350 mV overlapping with the oxidation peak of the adsorbed hydrogen strongly bounded to the Pt

surface. In is well known, that this peak belongs to the oxidation of tungsten bronze formed due to the hydrogen spillover. Cathodic counterpart (i.e. the current peak of the formation of the tungsten bronze) of this anodic peak coincides with the hydrogen-adsorption peaks of the platinum.

The average values of the ECSA (in m^2/g_{Pt}) obtained on fresh 40 wt.% Pt catalysts for three different batches increased in the following order: Pt/75$Ti_{0.93}Nb_{0.07}O_2$-25BP (49.7±2.7) < Pt/25$Ti_{0.93}Nb_{0.07}O_2$-75V (50.4±1.2) < Pt/$NiWO_4$-GNP (65.3±2.0). It should be noted that obtaining reproducible results in the study of 40 wt.% Pt electrocatalysts is a rather difficult task (all measurements were repeated at least four to six times until reproducible results are obtained): the average ECSA value obtained on fresh reference 40 wt.% Pt/C in four parallel CV measurements was 44.3 ± 3.1 m^2/g_{Pt}.

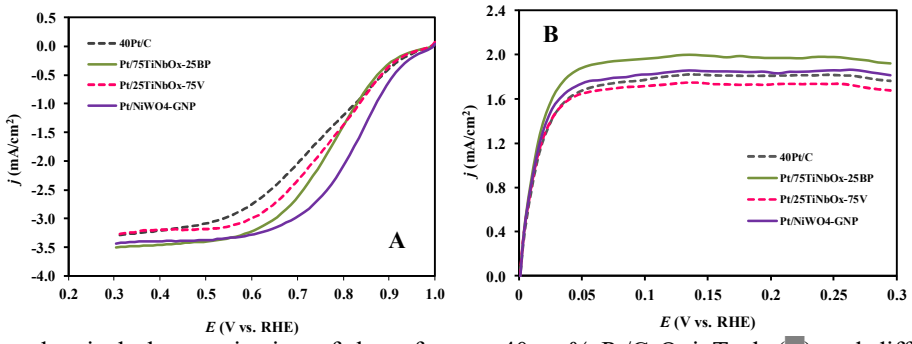

Fig. 11. Electrochemical characterization of the reference 40 wt.% Pt/C QuinTech ( ) and different 40 wt.% cathode electrocatalysts by RDE measurements at 900 rpm: Pt/75$Ti_{0.93}Nb_{0.07}O_2$-25BP ( ), Pt/25$Ti_{0.93}Nb_{0.07}O_2$-75V ( ) and Pt/$NiWO_4$-GNP ( ). (A) ORR curves obtained in O_2-saturated 0.5 M H_2SO_4; (B) HOR curves obtained in a H_2-saturated 0.5 M H_2SO_4. Obtained at 10 mV s^{-1}, T = 25 °C.

As shown in Figure 11.A the onset potential of the ORR on the reference Pt/C and both Nb-containing catalysts was observed at slightly less positive potential comparing to the Pt/$NiWO_4$-GNP, indicating that these catalysts are less active. Moreover, the mixed kinetics-diffusion control region of the $NiWO_4$-based catalyst is in the range from 0.6 V and 1.0 V, demonstrating that this catalyst performs well in the ORR. It can be seen from Fig. 11.B that the electrochemical performance of all mixed oxide-containing electrocatalysts in the HOR was very similar, while the Pt/75$Ti_{0.93}Nb_{0.07}O_2$-25BP catalyst shows a slightly higher activity.

In this series of experiments, the highest ECSA value and the best activity in the ORR was obtained on the Pt catalyst supported on the composites of Ni-based materials with GNPs prepared using direct synthesis method (see Fig. 11.A). However, preliminary results of our research group obtained using these catalysts as the cathode for a PEM fuel cell showed that the performance of the Pt/$NiWO_4$-GNP catalyst was worse in comparison with the optimal values. The presence of GNP in the catalyst may require more careful formulation of the ink composition to ensure good activity in fuel cell- these studies are currently ongoing.

The activity of both Nb-containing catalysts was quite comparable. Thus, the Pt/75$Ti_{0.93}Nb_{0.07}O_2$-25BP catalyst with high mixed oxide content was selected for the testing in portable fuel cell.

2.4.3 Alternative platinum loading process

It should be noted that we also tried to increase to 1 g the amount of the composite support used to load Pt in one batch. For this purpose, five consecutive steps were used to introduce Pt: the calculated amount of the Pt precursor compound ($H_2PtCl_6 \times 6H_2O$, required to prepare catalysts with the desired Pt content (e.g., 20 wt.%)) was divided into five equal portions and re-introduced into a round bottom flask containing 1 g of support material after the filtration and washing stage (see flow chart in Fig. 12).

After addition of new portion of the Pt precursor compound all steps of platinum loading process (see Fig. 12) were repeated again. After finishing of the last Pt deposition step, the catalyst was again washed four times with 50 ml water and filtered by centrifugation in order to remove the chloride ions and dried at 85 °C in an oven overnight. Detailed characterization of the catalyst prepared using consecutive deposition is in progress.

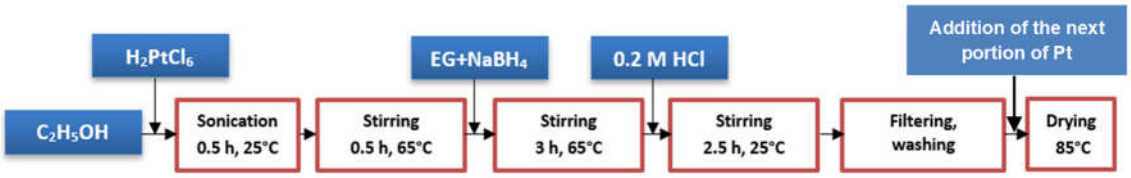

Fig. 12. Flow chart of the platinum loading process, including the consecutive steps of the introduction of Pt.

2.5 Catalyst layers deposition and standard single cell testing

Selection of the most promising catalyst compositions for testing in single fuel cell was done based in the results of obtained in a standard three-electrode electrochemical cell.

2.5.1 Catalysts inks preparation and MEAs preparation

In the reproducible manufacturing of the MEAs, a protocol was developed for the spray coating method, in which catalyst ink was painted by airbrush (AB200) onto the surface of gas diffusion layers (GDLs). Commercial 20 and 40 wt.% Pt/C QuinTech catalysts were used to optimize the MEA Pt content. The MEA comparison was carried out in accordance with the EU's harmonized New European Driving Cycle (NEDC) protocol. The optimal characteristics (1 A/cm^2 at 0.65 V) of the reference MEA with a power-proportional Pt load of 0.27 g_{Pt}/kW were achieved using 0.15 and 0.05 mg_{Pt}/cm^2 at the cathode (***c:*** 40 wt.% Pt/C) and anode (***a:*** 20 wt.% Pt/C), respectively.

Table 4. Characteristics of electrodes and MEAs used in standard single fuel cell testing

Electrodes & MEA	**Nominal composition of the electrocatalysts & Pt loading**
Anode vs. commercial Cathode	
Anode	20 wt.% Pt/25 wt.% $Ti_{0.8}Mo_{0.2}O_2$-75 wt.% BP 20 wt.% Pt/25 wt.% $Ti_{0.8}Mo_{0.2}O_2$-75 wt.% F-BP 20 wt.% Pt/25 wt.% $Ti_{0.8}Mo_{0.2}O_2$-75 wt.% V
Anode Pt loading, mg_{Pt}/cm^2	0.05
Commercial cathode	40 wt.% Pt/C (QuinTech)
Cathode Pt loading, mg_{Pt}/cm^2	0.15
Cathode vs. Anode	
Cathode	40 wt.% Pt/75 wt.% $Ti_{0.93}Nb_{0.07}O_2$-25 wt.% BP 40 wt.% Pt/25 wt.% $Ti_{0.93}Nb_{0.07}O_2$-75 wt.% V 40 wt.% Pt/$NiWO_4$-GNP
Cathode Pt loading, mg_{Pt}/cm^2	0.15
Anode	20 wt.% Pt/25 wt.% $Ti_{0.8}Mo_{0.2}O_2$-75 wt.% V
Anode Pt loading, mg_{Pt}/cm^2	0.05
MEA	**Preparation details**
Substrate	Teflon loaded carbon paper (H23C6, Freudenberg FCCT)
Ionomer 5% Nafion® dispersion	Nafion (D520, DuPont), 30 wt.% of catalyst layer; catalyst/dry Nafion= 2:1 mass ratio
Deposition method	spray coating by airbrush (AB200)
Membrane	Nafion XL (Ion Power)

Upon the catalyst ink preparation the variable parameters were the catalyst to ionomer ratio, the type and amount of solvent, Pt content of catalysts, Pt loading of GDEs, mode of the homogenization of catalyst ink. The mass ratio of the catalyst to dry Nafion is 2:1. The solvent is isopropanol which is applied in the same volume as Nafion solution. The calculated loss is 60%. Characteristics of electrodes included the nominal composition of the electrocatalysts and MEAs used in standard single fuel cell testing was presented in Table 4.

2.5.2 Single cell assembly and testing under standard conditions

20 wt.% Pt/25$Ti_{0.8}Mo_{0.2}O_2$-75C (C: BP, F-BP, V) anode catalysts

Based on the half-cell results three TiO_2-rutile-based 20 wt.% Pt/25$Ti_{0.8}Mo_{0.2}O_2$-75C (C: Vulcan (V), unmodified (BP) and functionalized Black Pearls 2000 (F-BP)) catalysts with $Ti_{0.8}Mo_{0.2}O_2$/C= 25/75 mass ration were chosen for the anode side (***a***: 0.05 mg_{Pt}/cm^2), while commercial 40 wt.% Pt/C was applied as cathode (***c***: 0.15 mg_{Pt}/cm^2). As shown in Fig. 13 the best performance and the lowest ohmic resistance were observed on the Vulcan-containing composite supported Pt catalyst. However, the BP-based catalyst demonstrated better stability.

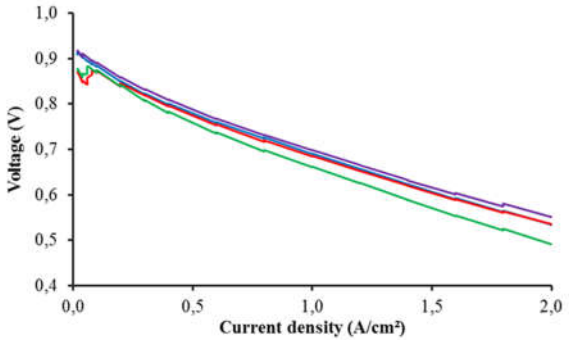

Fig. 13. Polarization responses for 0.05 mg Pt/cm^2 loaded Pt/25$Ti_{0.8}Mo_{0.2}O_2$-75C anode catalysts (C: unmodified BP ( ) and functionalized BP (F-BP:) and Vulcan ( )). Results obtained on the commercial 20 wt.% Pt/C QuinTech ( ) catalyst used at the anode side are given for comparison.

40 wt.% Pt cathode electrocatalysts

40 wt.% Pt electrocatalysts with 0.15 mg_{Pt}/cm^2 loading supported on 75$Ti_{0.93}Nb_{0.07}O_2$-25BP, 25$Ti_{0.93}Nb_{0.07}O_2$-75V and Pt/$NiWO_4$-GNP composites were tested on the cathode side (see Table 4 and Fig. 14); in all these MEAs the best 20 wt.% Pt/25$Ti_{0.8}Mo_{0.2}O_2$-75V (0.05 mg_{Pt}/cm^2) was used at the anode side. Compositions of the MEA used in standard single cell testing were presented in Table 4. Despite the fact that the optimized loading of Pt was used, the characteristics of the Pt/$NiWO_4$-GNP catalyst, obtained under standard conditions, are somewhat worse in comparison with the optimal values. The best performance was observed on the Pt/25$Ti_{0.93}Nb_{0.07}O_2$-75V catalyst.

Activity increased in the following order:

40 wt.% Pt/$NiWO_4$-GNP < 40 wt.% Pt/75$Ti_{0.93}Nb_{0.07}O_2$-25BP < 40 wt.% Pt/25$Ti_{0.93}Nb_{0.07}O_2$-75V.

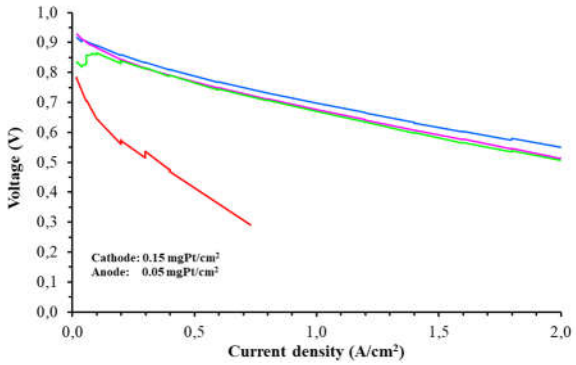

Fig. 14. Polarization responses for 0.15 mg Pt/cm^2 loaded cathode catalysts: 40 wt.% Pt/75$Ti_{0.93}Nb_{0.07}O_2$-25BP ( ), 40 wt.% Pt/25$Ti_{0.93}Nb_{0.07}O_2$-75V ( ) and 40 wt.% Pt/$NiWO_4$-GNP ( ). Results obtained on reference 40 wt.% Pt/C ( ) catalyst are given for comparison. In all cases 20 wt.% Pt/25$Ti_{0.8}Mo_{0.2}O_2$-75V catalyst was used on anode side (see Table 4).

Changes in the electrochemically active Pt surface area occurring during the Dynamic Load Cycle (DLC) test were studied by CV measurements done on fresh and aged MEAs. The investigation of the morphology of the catalyst-loaded GDL before and after fuel cell testing by SEM-EDX is in progress.

2.6 Design, preparation and testing in portable fuel cell and stack

2.6.1 Single portable fuel cell

First, portable single PEMFCs and stacks operating under full passive conditions (air-breathing cathode and full dead-end anode) was mounted and tested by Spanish subcontractor (**CIEMAT**) using commercial gas diffusion electrodes (cathode: FCETC (0.30 mgPt/cm^2 40 wt.% Pt/C on carbon cloth); anode: E-TEK (0.25 mgPt/cm^2 on carbon cloth)).

Some cell details are presented in Fig. 15, where Fig. 15.a shows the components of the circular cell, whereas Fig. 15.b shows a photograph of the cell with 3 cm diameter active area and 5 cm total diameter. The circular shape helps homogeneity of current generation and gas tightness. Plates, contacts, and gaskets, were fabricated in the workshops of **CIEMAT**. Silicone gaskets are used for gas tightness in the anode. The portable cell is able to operate under full passive conditions during hours, without purging, which allows for 100% faradaic efficiency. The basic ideas of the cells were patented by Spanish subcontractor before the project started.

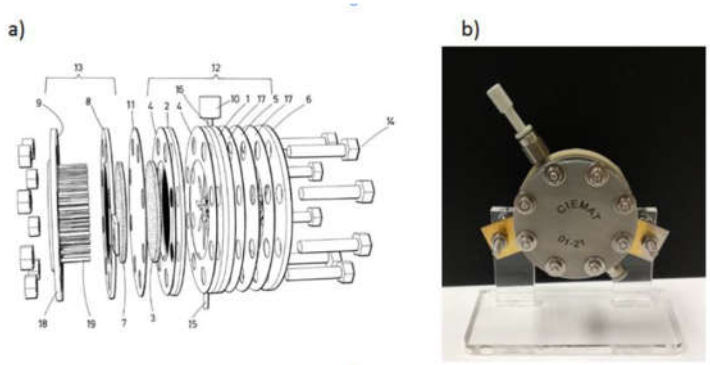

Fig. 15. (a) Exploded view of the portable, air-breathing fuel cell: an air breathing cathode (13); a passive, dead-end, anode (12); a columnar end-plate of the air breathing cathode (18,19); a gold coated grid contact (8) for collecting the current from the cathodic gas diffusion electrode (7); Nafion NR 212 as electrolyte membrane (11); the anode is dead-end, using a hydrophilic back membrane for water rejection (5), and a similar grid contact (2) for current collection; all the components are fixed with eight bolts and nuts (14). **(b)** Photograph of the cell (3 cm active area diameter, 5 cm total diameter).

The single cell with 7 cm^2 is able to deliver up to 1.2 W under pure passive conditions: fed with static hydrogen (0.5 bar) and ambient air (23 °C, 30% RH). The single cell in Fig. 16 is intended for small portable application when fed with a portable hydrogen storage system (Fig. 16.a). By using a metal-hydride cartridge (Horizont, 1 g H_2) the portable power system is complete and can be compared with other portable power generators like batteries.

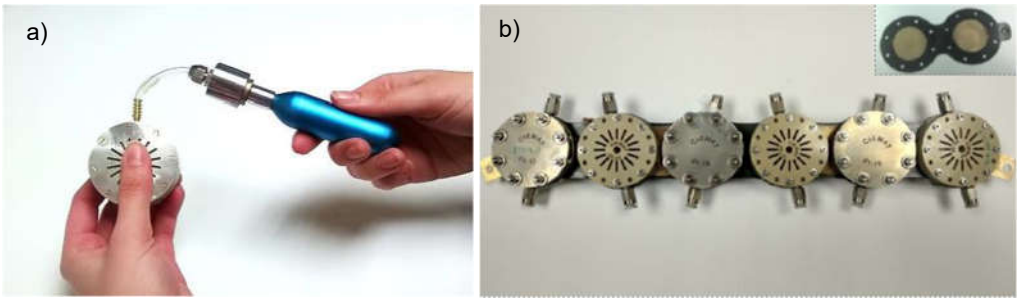

Fig. 16. (a) Portable hydrogen fuel cell system with single cell described and metal-hydride hydrogen canister (1 g H_2, 100 g total weight); **(b)** planar stack. Inset: grid contact for serial connection.

Impedance spectroscopy shows ohmic losses and transport limitations larger than in conventional PEMFCs. The ohmic losses are attributed to the low working temperature (40 °C) and dry gas feeding. Transport limitations at high current generation rate (low cell voltage) are due to passive liquid water elimination from the cathode.

2.6.2 Portable fuel cell stack

Single cells can be stacked to produce any desired power. A 6-cell stack in a planar configuration was built from the serial connection of portable single cells (see Fig. 16.b). The stack delivers 5 W under portable conditions (no convective flows). Power production is below the nominal 7 W due to some inefficiency by the stacking the cells: the main losses by stacking occur mainly in the resistance of contacts between cells and in the higher dissipation of heat. These inefficiencies are currently being working out. When supplied from a hydrogen canister (1 g H_2), the stack is able to produce electricity for more than 2.5 hours without purging; the steady-state temperature is attained at 37°C. As shown in Fig. 17.a, larger stacks, composed of two sets of 7 serial cells connected in parallel, were also mounted and tested. This stack provides continuous 14 W and is intended for connection to an electronic with supercapacitors energy storage, able to provide up to 50 W transient power (Fig. 17.b). The whole system is intended for small portable applications where peaks of power are required during limit time (Fig. 17.b), and continuous low power production.

Main characteristics of the portable power production by single cells and stacks can be summarized as follows: (i) static hydrogen and air feedings, (ii) 100% faradaic efficiency (no purging), (iii) no active cooling required, (iv) no fans nor moving parts, (v) complete silent operation, (vi) total modularity and single cell accessibility, (vii) flexible connectivity: serial/parallel, (viii) multiple stacking possibilities: linear, planar, volume.

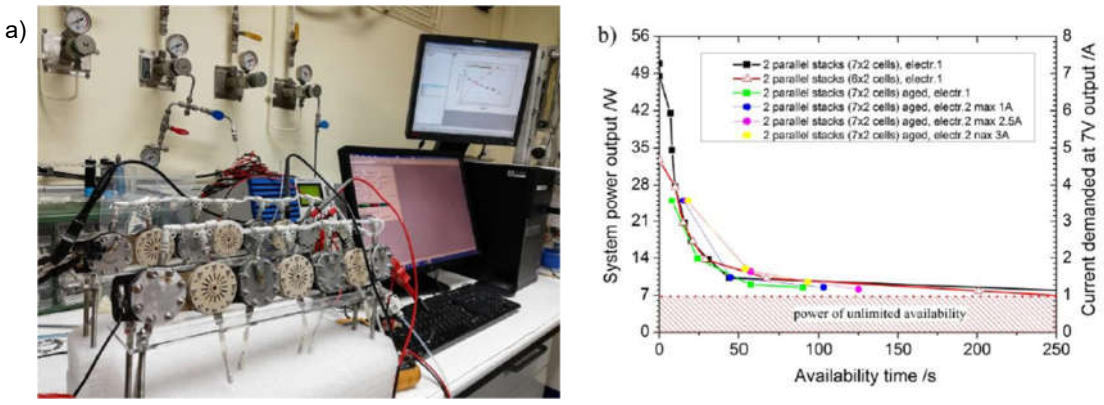

Fig. 17. (a) Portable stack composed of two 7 serial cells connected in parallel; **(b)** transient power output characteristics of the stack with supercapacitors energy storage.

2.6.3 Testing of the best catalysts in portable fuel cell

Table 5. Prepared electrodes characteristics and commercial reference electrodes used for portable fuel cell testing

Electrode	**Anode**	**Cathode**
anode vs. commercial cathode		
Catalyst	20 wt.% Pt/25$Ti_{0.8}Mo_{0.2}O_2$-75BP	40 wt.% Pt/C (FCSTORE)
Pt loading, mg_{Pt}/cm^2	0.03	0.3
Substrate	carbon cloth ELAT	carbon cloth
cathode vs. commercial Anode		
Catalyst	40 wt.% Pt/C (FCSTORE)	40 wt.% Pt/75$Ti_{0.93}Nb_{0.07}O_2$-25BP
Pt loading, mg_{Pt}/cm^2	0.03	0.3
Substrate	carbon cloth	carbon cloth ELAT
commercial anode vs. commercial cathode		
Catalyst	40 wt.% Pt/C (FCSTORE)	40 wt.% Pt/C (FCSTORE)
Pt loading, mg_{Pt}/cm^2	0.03	0.3
Substrate	carbon cloth	carbon cloth

Ionomer: Nafion 212NR (30 wt.% of catalyst layer); active area size: 12.6 cm^2; shape: circular.

Based on the half-cell results, three anode and three cathode catalysts were selected as the best catalysts for the investigation in PEM fuel cell: each catalyst has its own advantages.

Currently, measurements have been carried out in portable fuel cell using one anode (20 wt.% $Pt/25Ti_{0.8}Mo_{0.2}O_2$-75BP) and one cathode (40 wt.% $Pt/75Ti_{0.93}Nb_{0.07}O_2$-25BP) catalysts. Characteristics of prepared electrodes used for portable fuel cell testing are shown in Table 5.

Polarization curves of the three portable cells configurations are shown in Fig. 18. The portable cell results show lower performance with the cathode catalyst compared with the reference cell. The results show initially lower performance of anode catalyst, than the reference cell. No decay is observed in the cells under operation, until 24 h of continuous work. The anodic catalyst cell increases performance slightly (limiting current), and shows similar behavior as the reference cell. It should be noted, the lower temperature (40 °C) of portable cells and dry gas feeding conditions may favor the better stability of the cells compared with the standard PEM fuel cells.

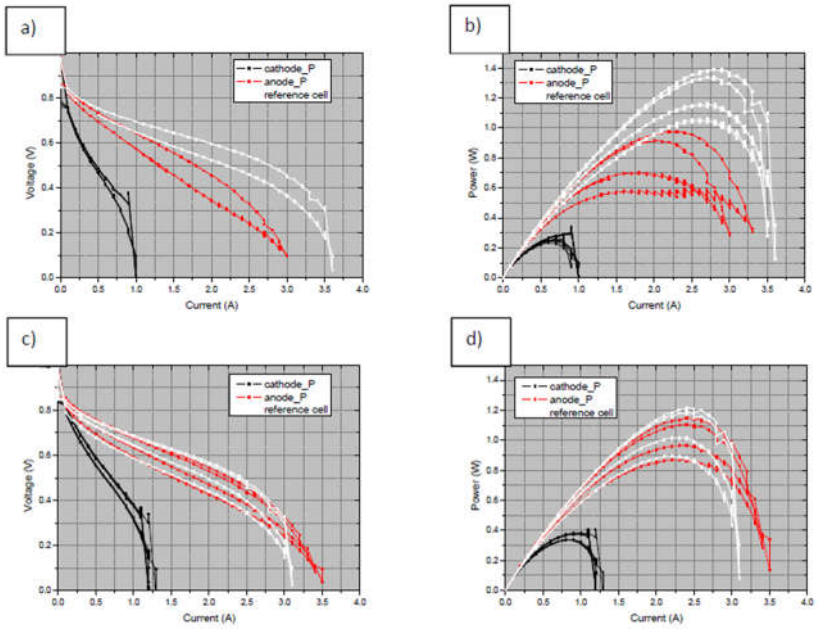

Fig. 18. Polarization curves (a, c), and power curves (b, d) of initial cell (a, b) and cells after 24 h operation (c, d).

The internal resistance, measured for the cells by the current step method, increased in the following order: reference cell: (273 mOhm·cm^2) < anodic catalyst cell (590 mOhm·cm^2) < cathodic catalyst cell (690 mOhm·cm^2).

3. Utilization possibilities of the results

Fuel cells are devices that transform efficiently the chemical energy of hydrogen into clean electricity. The fuel cell technology is attractive for its high-energy efficiency and it became very relevant in the last decade. Moreover, the utilization of fuel cells for portable electronic devices has seen remarkable increase in the last few years. Performances of fuel cells, among other factors, strongly depend on the types of electrocatalysts. Therefore, our results can contribute to the production of more economic and more durable fuel cells and through this can contribute for a sustainable future.

The work performed within this project clearly pointed out the added value of the complementary competences of the Hungarian, Romanian and Spanish partners. We definitely plan further collaboration, involving further proposals, based on this complementarity.

Based on our results, we plan to submit a patent. KONTAKT Elektro GmbH (Pécs, Hungary), which also produces and distributes fuel cells, expressed interest in our new type of catalysts, while STIMPEX S.A. in Romania expressed interest in using the results of the project regarding to portable fuel cell and stack.

4. Changes in research staff and other relevant information

The research proceeded according to the work plan presented in the proposal. Danielle Verde Nolasco in the 2nd year of the project and Khirdakhanim Salmanzade in the 2nd and the 3rd years of the

project were employed as young researchers. Danielle Verde Nolasco task was helping in the catalyst layers deposition, MEAs preparation and standard single fuel cell testing. Khirdakhanim Salmanzade task was helping in the electrochemical characterization of the large number of samples prepared by **P1** and **P2** as well as the preparation and characterization of Sn-containing composite supported Pt catalysts. During the 3rd years of the project, Asmaa Khaled Mohamed Selim (PhD, research fellow) was involved in characterization of the MEAs in fuel cells. There was no other personal change.

Dr. András Tompos (PI) and Dr. Irina Borbáth (Key Person) met with Romanian partners in Bucharest on June 5-7, 2019. From Romanian side the project manager of **P2** Dr. Simona Somacescu visited Budapest on November 26-28, 2019. In 2021, due to the outbreak of COVID-19, partners were unable to travel, but the exchange of samples for electrochemical and physicochemical characterization was done by mail. In 2022, the project manager of **P3** Dr. Mihaela Florea visited Budapest in March and during the visit to the conference in Bale Govora (13th International Symposium of the Romanian Catalysis Society, June 22-24, 2022, Romania) there was also an opportunity to discuss the obtained results and the work plan for the future.

5. References

1. Ș. Neațu, F. Neațu, I. M. Chirica, I. Borbáth, E. Tálas, A. Tompos, S. Somacescu, P. Osiceanu, M. A. Folgado, A. M. Chaparro, M. Florea: „Recent progress on electrocatalysts and electrodes for portable fuel cells." **Journal of Materials Chemistry A,** 9 (2021) 17065. DOI: 10.1039/D1TA03644K
2. S. Somacescu, P. Osiceanu, J. M. Calderon Moreno, D. C. Culita, F. Neațu, M. M. Trandafir, Ș. Neațu, A. Kuncser, G. P. Szijjártó, E. Tálas, A. Tompos, I. Borbáth, M. Florea: „Design of electrocatalysts with reduced Pt content supported on mesoporous $NiWO_4$ and $NiWO_4$-graphene nanoplatelets–composite for oxygen reduction and hydrogen oxidation in acidic medium." **International Journal of Hydrogen Energy** Accepted 26 April 2022, https://doi.org/10.1016/j.ijhydene.2022.04.270
3. I. Borbáth, E. Tálas, Z. Pászti, K. Zelenka, I. Ayyubov, K. Salmanzade, I. E. Sajó, Gy. Sáfrán, A. Tompos: "Investigation of Ti-Mo mixed oxide-carbon composite supported Pt electrocatalysts: Effect of the type of carbonaceous materials." **Applied catalysis A- General**, 620 (2021) 118155. https://doi.org/10.1016/j.apcata.2021.118155
4. I. Borbáth, K. Zelenka, Á. Vass, Z. Pászti, G.P. Szijjártó, Z. Sebestyén, G. Sáfrán, A. Tompos: "CO tolerant Pt electrocatalysts for PEM fuel cells with enhanced stability against electrocorrosion." **International Journal of Hydrogen Energy**, 46 (2021) 13534-13547. https://doi.org/10.1016/j.ijhydene.2020.08.002
5. I. Ayyubov, I. Borbáth, Z. Pászti, Z. Sebestyén, J. Mihály, T. Szabó, E. Illés, A. Domján, M. Florea, D. Radu, A. Kuncser, A. Tompos, E. Tálas: "Peculiarities of graphite oxide derived TiO_2-carbon composites as electrocatalyst supports for polymer electrolyte membrane fuel cells." **Topics in Catalysis**, 2021, https://doi.org/10.1007/s11244-021-01513-1
6. E. Tálas, I. Ayyubov, A. Vulcu, C. Berghian-Grosan, I. Borbáth, Z. Pászti, Gy. Sáfrán, J. Mihály, Á. Szegedi, A. Tompos: „Use of the ball milling technique in the preparation of potential catalysts for polymer electrolyte membrane fuel cells (PEMFC)". **Book of abstract RomCat 2022** (13th International Symposium of The Romanian Catalysis Society, June 22-24, 2022, Baile Govora, Romania), pp. 21-22.
7. I. Borbáth, K. Salmanzade, E. Tálas, Z. Pászti, K. Zelenka, I. Ayyubov, C. Silva, G. Sáfrán, I.E. Sajó, A. Tompos: „Requirements for multifunctional composite supports and electrocatalysts to achieve high CO tolerance and stability". **Book of abstract RomCat 2022** (13th International Symposium of The Romanian Catalysis Society, June 22-24, 2022, Baile Govora, Romania), pp. 19-20.
8. C. Silva, I. Borbáth, K. Zelenka, I. E. Sajó, G. Sáfrán, A. Tompos, Z. Pászti: "Effect of the reductive treatment on the state and electrocatalytic behavior of Pt in catalysts supported on $Ti_{0.8}Mo_{0.2}O_2$–C composite." **Reaction Kinetics, Mechanisms and Catalysis,** 135 (2022) 29–47. Open Access. https://doi.org/10.1007/s11144-021-02131-4
9. I. Borbáth, K. Salmanzade, E. Tálas, Z. Pászti, C. Silva, I.E. Sajó, S. Neatu, A. Kuncser, D. Radu, M. Florea, A. Tompos: „Design of Ti–Sn mixed oxide–carbon composite supports for Pt-based electrocatalysts for polymer electrolyte membrane fuel cells: peculiarities of preparation." **Book of**

abstract RomCat 2022 (13th International Symposium of The Romanian Catalysis Society, June 22-24, 2022, Baile Govora, Romania), pp. 17-18.

10. I. Ayyubov, E. Tálas, K. Salmanzade, A. Kuncser, Z. Pászti, Ș. Neațu, A.G. Mirea, M. Florea, A. Tompos, I. Borbáth: „Electrocatalytic Properties of Mixed-Oxide-Containing Composite-Supported Platinum for Polymer Electrolyte Membrane (PEM) Fuel Cells." **Materials**, 2022, 15, 3671. https://doi.org/10.3390/ma15103671